Dalton Transactions

ROYAL SOCIETY OF CHEMISTRY

COMMUNICATION

View Article Online
View Journal | View Issue

Cite this: *Dalton Trans.*, 2023, **52**, 9541

Received 28th April 2023,
Accepted 29th June 2023

DOI: 10.1039/d3dt01284k

rsc.li/dalton

Tetranuclear Ru_2Cu_2 and Ru_2Ni_2 complexes with nanomolar anticancer activity†

Andrés Alguacil,[a] Franco Scalambra,[a] Pablo Lorenzo-Luis,[b,c] Adrián Puerta,[b] Aday González-Bakker,[b] Zenaida Mendoza,[a,c] José M. Padrón[b] and Antonio Romerosa*[a]

Complexes [{RuCp(PPh$_3$)$_2$-μ-dmoPTA-1κ*P*:2κ^2-*N*,*N*′-CuCl}$_2$-μ-Cl-μ-OCH$_3$](CF$_3$SO$_3$)$_2$·(CH$_3$OH)$_4$ (1) and [{RuCp(PPh$_3$)$_2$-μ-dmoPTA-1κ*P*:2κ^2-*N*,*N*′-NiCl}$_2$-μ-Cl-μ-OH](CF$_3$SO$_3$)$_2$ (2) have been synthesized and characterized. Their antiproliferative activities were assessed against six human solid tumours showing nanomolar GI$_{50}$ values. The effects of 1 and 2 on SW1573 cells colony formation, HeLa cells action mechanism and their interaction with the pBR322 DNA plasmid were evaluated.

Since the discovery of cisplatin antiproliferative properties in 1965,[1] platinum complexes have been extensively studied as anticancer agents. Nevertheless, the side effects provoked by the general low selectivity of this class of compounds,[2] prompted the research community to investigate alternatives. Ru-based compounds are thought of as promising substitutes to platinum drugs due to their adequate ligand exchange kinetics, the ability of Ru to mimic iron in biological systems and its high number of accessible oxidation states.[3] Different families of ruthenium compounds have been synthesized achieving great advances and even entering clinical trials such as *trans*-[RuCl$_4$(DMSO)Im][ImH] (NAMI-A),[3,4] or Ru-arene complexes (RAPTA) that show interesting pharmacological profiles.[5,6]

We started an in-depth study on RuCp complexes families bearing the ligands mPTA and dmoPTA (mPTA = *N*-methyl-1,3,5-triaza-7-phosphaadamantane, dmoPTA = 3,7-dimethyl-1,3,7-triaza-5-phosphabicyclo[3.3.1]nonane) some years ago,[7–9] these complexes displaying medium to high antiproliferative activities mostly with the ligand dmoPTA.[10–17] Additionally, we developed a family of complexes with the general formula [RuCp(L)(PPh$_3$)-μ-dmoPTA-1κ*P*:2κ^2*N*,*N*′-E] (L = Cl, PPh$_3$; E = H, ML′$_2$, M = Zn, Ni, Co; L′ = Cl, acac) that evidenced the usefulness of incorporating a second metallic unit. The best antiproliferative activity was shown by the complex [RuCp(PPh$_3$)$_2$-μ-dmoPTA-1κ*P*:2κ^2*N*,*N*′-ZnCl$_2$](CF$_3$SO$_3$), together with certain selectivity against tumoral cells.[18] To continue this study, we decided to coordinate CuCl$_2$ and NiCl$_2$ fragments to the [RuCp(PPh$_3$)$_2$(dmoPTA)]$^+$ scaffold. This choice was born from the importance of these two metals in various biochemical processes: copper is an essential trace element,[19] and is involved in primary processes being fundamental for scavenging harmful reactive oxygen species.[20,21] Similarly, nickel is another essential element for life, playing important roles in some metalloenzymes such as urease,[22] as Ni(II) can coordinate with the N7 of adenine and guanine and stabilize RNA and DNA.[23,24]

This paper presents the reactivity of [RuCp(PPh$_3$)$_2$-κ*P*-dmoPTA](CF$_3$SO$_3$) with CuCl$_2$ and NiCl$_2$. The obtained tetrametallic compounds were characterized and their antiproliferative activities were tested against a panel of cancer cells. Finally, to shed light on the action mechanism of these complexes, their apoptotic profile was studied using label-free live cell imaging and their reactivity was tested against DNA. Obtained results show how these polymetallic complexes display exceptional nanomolar anticancer activity.

Reacting one equivalent of CuCl$_2$·2H$_2$O with [RuCp(PPh$_3$)$_2$(dmoPTA)](CF$_3$SO$_3$) in MeOH, crystals of the tetrametallic complex [{RuCp(PPh$_3$)$_2$-μ-dmoPTA-1κ*P*:2κ^2-*N*,*N*′-CuCl}$_2$-μ-Cl-μ-OCH$_3$](CF$_3$SO$_3$)$_2$·(CH$_3$OH)$_4$ (**1**) were obtained (Scheme 1). Similar tetrametallic complex [{RuCp(PPh$_3$)$_2$-μ-dmoPTA-1κ*P*:2κ^2-*N*,*N*′-NiCl}$_2$-μ-Cl-μ-OH](CF$_3$SO$_3$)$_2$ (**2**), but with Ni instead of Cu, was synthesized by reaction of starting complex with two equivalents of NiCl$_2$·6H$_2$O in an ethanolic solution (Scheme 1).

Despite the paramagnetic character of Cu(II) and Ni(II) metals, the distinctive resonances of the PPh$_3$ and dmoPTA ligands were observed in the ^{31}P{^{1}H} NMR spectra of

[a]*Área de Química Inorgánica-CIESOL, Universidad de Almería, 04120 Almería, Spain. E-mail: romerosa@ual.es*
[b]*BioLab, Instituto Universitario de Bio-Orgánica "Antonio Gónzalez", Universidad de La Laguna, C/ Astrofísico Francisco Sánchez 2, 38071 La Laguna, Spain*
[c]*Área de Química Inorgánica, Departamento de Química, Universidad de La Laguna, C/ Astrofísico Francisco Sánchez 3, 38071 La Laguna, Spain*

†Electronic supplementary information (ESI) available. CCDC 2245836 and 2245837. For ESI and crystallographic data in CIF or other electronic format see DOI: https://doi.org/10.1039/d3dt01284k

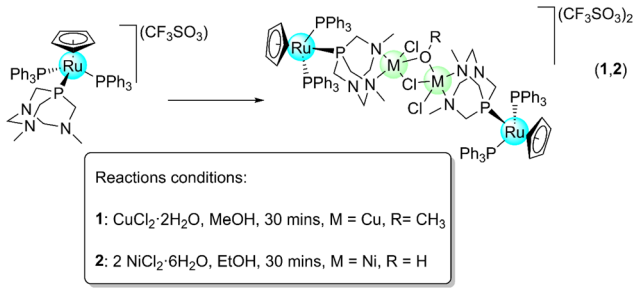

Scheme 1 Synthesis of **1** and **2**.

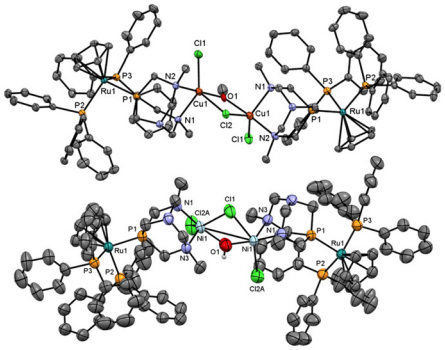

Fig. 1 Thermal ellipsoid representation (50%) of the complex unit in the crystal structures of **1** (up) and **2** (bottom). Anions and solvent molecules have been omitted for the sake of clarity.

complexes **1** and **2**. For concern **1**, two broad signals were found (Fig. S3†) in its $^{31}P\{^1H\}$ spectrum: one ascribable to PPh_3 (δ_{CDCl_3}: 37.94 ppm) and the other to dmoPTA (δ_{CDCl_3}: −43.58 ppm). In the case of **2**, in $CDCl_3$ two distinct sets of resonances in a 2 : 1 ratio were observed, which are constituted by a doublet and a broad triplet: the signals arising at 38.39 ppm (d) and −13.72 ppm (bt), arise at the same chemical shift that those for the PPh_3 and HdmoPTA of the complex $[RuCp(PPh_3)_2(HdmoPTA)]^{2+}$,[16] while the resonances at 36.83 ppm (d) and 133.47 ppm (bt) could be ascribable to a bimetallic derivative where Ni is coordinated to the dmoPTA ligand. Both complexes **1** and **2** present two triflate anions as counterions, whose presence was confirmed by IR spectroscopy by the $\nu(SO_3)$ band (**1**: 1268 cm^{-1}; **2**: 1259 cm^{-1}), which is in the expected range for the triflate anion and similar to that of the starting compound (1274 cm^{-1}).[16]

To determine the behaviour of the obtained complexes in solution, ^1H DOSY NMR experiments were carried out in $CDCl_3$, where they are enough soluble. The obtained results suggest that both have evolved in the corresponding bimetallic complexes, as proposed in Scheme 2. The presence of two species with slightly different hydrodynamic radii (hydrodynamic radii = 6.69(**1**) Å; 6.48(**2**) Å) was observed, which is similar to previously published bimetallic complexes containing dmoPTA.[25] Nevertheless, these experiments do not discard the possible presence of tetrametallic complexes in solution. It is significant to point out that NMR and IR studies as well as the obtained hydrodynamic radii (Table S1†) are compatible with the size of the two possible different bimetallic derivatives obtained from **1** and **2**: complexes **1a**, **1b**, **2a** and **2b** (Scheme 2).

Single crystals of complexes **1** and **2** were obtained in MeOH and EtOH. Their crystal structure (Fig. 1), their description and discussion, as well as the complete lists of bond lengths and angles, can be found in ESI.†

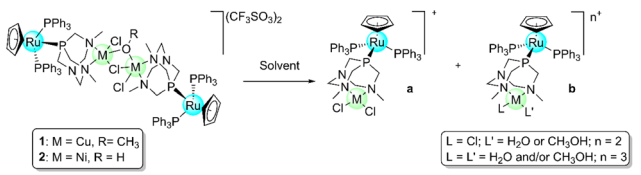

Scheme 2 Proposed decomposition of the dimetallic complexes **1** and **2** into **1a**, **1b**, **2a**, **2b** in solution.

Assessing the antiproliferative activity of the complexes requires dissolving them in a cell culture medium, which contains mainly water. Thus, the stability of **1** and **2** was monitored over time by $^{31}P\{^1H\}$ NMR at room temperature and 37 °C both in DMSO and DMSO/D_2O (1 : 1) mixture (Fig. S10–S17†).

The stability test of complex **1** in DMSO at room temperature (Fig. S10†) shows that noteworthy differences in the ratio of the intensities in the $^{31}P\{^1H\}$ NMR signals can be seen even after 1 h (Fig. S10, S11, S13, S16 and S17†) due to possible equilibria between different complexes, in which solvent molecules have substituted the labile chlorides. The same behaviour was observed at 37 °C (Fig. S11†), but the first evidence of product decomposition appears after 4 h. However, when the stability is tested in the DMSO-d_6/D_2O mixture (1 : 1), the complex is stable for 48 h both at room temperature and at 37 °C (Fig. S12 and S13†), where negligible decomposition signals (<4%) are observed.

Likewise, the $^{31}P\{^1H\}$ NMR spectra of complex **2** in DMSO-d_6 both at room temperature and 37 °C (Fig. S14 and S15†) does not change significantly after 48 h; only a few small new signals are observed after 24 h with intensities under 8%. In contrast, when stability is studied in the DMSO/D_2O mixture the signal relative to the dmoPTA ligand remains stable while those corresponding to PPh_3 vary their intensities over time both at room temperature and 37 °C (Fig. S16 and S17†). The NMR spectra of complexes **1** and **2** in DMSO-d_6/D_2O are different to those of the starting complex with $CuCl_2$ (Fig. S18†) and $NiCl_2$ (Fig. S19†). The presence of species containing dmoPTA-coordinated Cu(II) was confirmed also by UV-Vis measurements, which show at *ca.* 650 nm the typical amino-Cu(II) absorption (Fig. S20†) and by ESI-MS measurements (Fig. S22–S36†). Nevertheless, as mentioned before, considering the general lability of Cu(II) and Ni(II) complexes in dissolution, the presence of equilibria involving ligand–solvent exchange should not be discarded.

The initial assessment of the antiproliferative activity of complexes **1–2** was carried out in a panel of six human solid tumour cell lines using cisplatin (CDDP) as standard. The

Table 1 GI_{50} values (nM) of cisplatin, **1** and **2** against human solid tumour cell lines

	Cell lines					
	A549 (lung)	HBL-100 (breast)	HeLa (cervix)	SW1573 (lung)	T-47D (breast)	WiDr (colon)
CDDP[a]	4933 ± 180	1866 ± 162	1787 ± 518	2746 ± 375	16 846 ± 3258	22 978 ± 4316
$[RuCp(PPh_3)_2(dmoPTA)]^{+}$ [b]	140 ± 20	320 ± 30	190 ± 10	190 ± 50	330 ± 10	270 ± 30
1*	28 ± 3.3	32 ± 0.2	21 ± 1.7	27 ± 13	20 ± 7.8	21 ± 9.2
2*	34 ± 8.4	31 ± 11	28 ± 2.5	41 ± 6.8	23 ± 1.6	34 ± 8.7

[a] The GI_{50} values of CDDP were obtained for this work, being in agreement with those found in the literature.[26–28] [b] Ref. 18. *$CuCl_2{\cdot}2H_2O$ and $NiCl_2{\cdot}6H_2O$ cytotoxicity values found in the literature do not show values comparable to those obtained for **1** and **2**.[29–32]

results expressed as growth inhibition 50% (GI_{50}) after 48 h exposure, are shown in Table 1. Both complexes were able to induce cell growth inhibition at the nanomolar range in all cell lines. The GI_{50} values range between 20–32 and 23–41 nM for complexes **1**–**2**, respectively. The results represent an enhancement for the previously reported parent complexes, surpassing the most active complex synthesized by us so far in all the cell lines tested, except for the SW1573 cell line, which was more susceptible to the treatment with complex [RuCp$(PPh_3)_2$-μ-dmoPTA-1κ*P*:2κ^2*N*,*N*′-$ZnCl_2$][CF_3SO_3].[18]

Next, we studied the ability of complexes **1**–**2** to disturb the colony formation of SW1573 cells to evaluate the effects on cell aggregation over time (Fig. 2). Both compounds were assayed at two doses based on the GI_{50} values from Table 1: a high (GI_{50}) and a low (GI_{50}/3) dose. None of these molecules was able to decrease the number of colonies notoriously (Fig. 2A). Nevertheless, the number of cells in the aggregates was lower in the treated groups when compared to untreated cells, as determined by the optical density measurements of the stained colonies after the solution of the dye (Fig. 2B). Complex **1** decreased the size and density of the colonies. A similar effect was also observed for compound **2** (Fig. 2A).

Label-free live cell imaging allowed us to observe cellular responses to compounds **1**–**2** over time. With this technology, it is possible to assess differences in responses to treatments within a cell population. For instance, cell death is a process that rarely occurs as an instant event. HeLa cells were exposed to complexes **1**–**2** at 10 times the GI_{50} values, *i.e.* 200 and 300 nM, respectively. Fig. 3A depicts how both treatments with **1** and **2** induced apoptotic cell death in HeLa cells. The effect is broadly observed after 12 hours of exposure to the compounds. However, hints of these types of cell death are present 6 hours after exposure, with membrane blebbing and reduction of cell size compared to the untreated sample. Apoptotic induction was tracked over time using the live cell death assay, in which cell content and morphology parameters based on the refractive index are integrated to evaluate cell status. As seen in

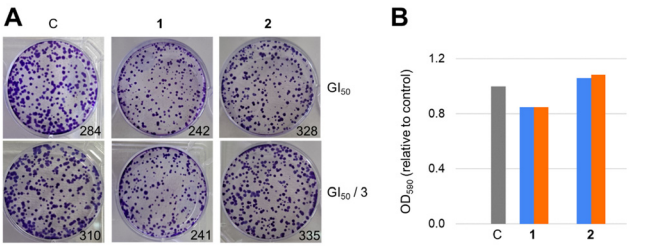

Fig. 2 Colony formation assay of SW1573 cells exposed to complexes **1**–**2**. (A) Representative crystal violet staining of the colonies formed after seven days of incubation and the number of colonies counted under respective conditions. (B) Relative optical density of crystal violet content of the treatments concerning control cells (C) at high (left bar) and low (right bar) doses.

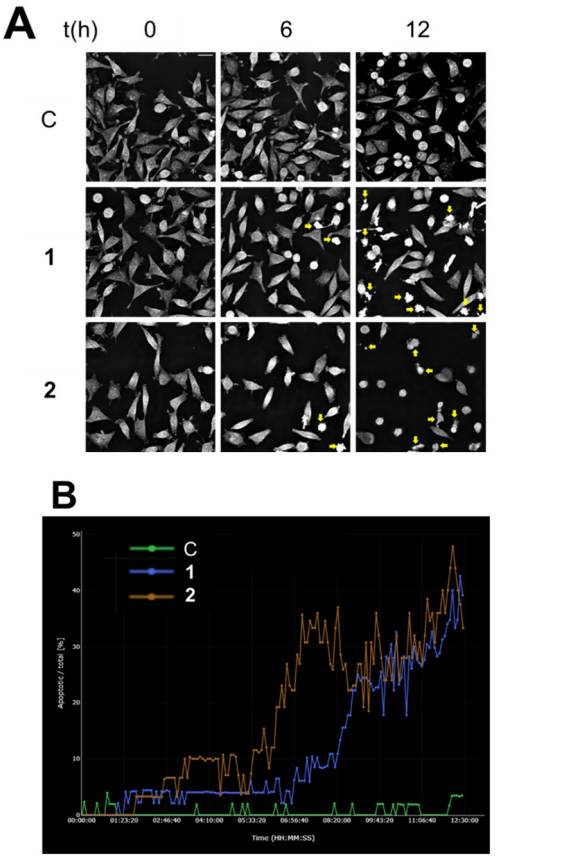

Fig. 3 (A) Representative images of live cell imaging assay on HeLa cells using 200 and 300 nm of **1** and **2** respectively. Yellow arrows point to apoptotic cells. (B) Kinetics of apoptotic cells obtained with the live cell death assay after live microscopy observations, the total exposure time was 12 hours. Green: untreated cells (C). Blue **1** (200 nM). Orange: **2** (300 nM).

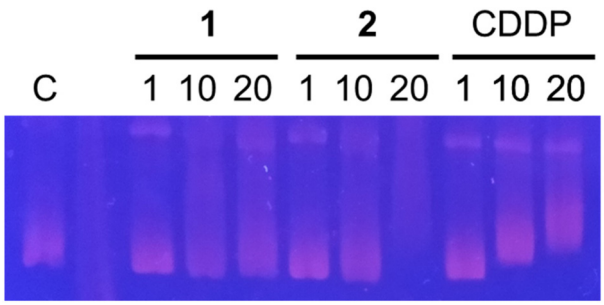

Fig. 4 Agarose gel electrophoresis of pBR322 plasmid DNA (C, control) incubated at 37 °C for 24 with **1**, **2** and CDDP at the indicated concentrations.

Fig. 3B, apoptosis is induced by both compounds, matching the visual inspection of the samples under every treatment. Cells treated with **2** entered faster in apoptosis before 7 hours, and close to 50% of the population showed apoptotic phenotypes after treatment when compared to 40% for treatment with compound **1**.

Finally, we tested the reactivity of complexes **1–2** with pBR322 DNA plasmid by gel electrophoresis (Fig. 4) according to established procedures,[33] using cisplatin as a reference. Compounds **1–2** did not alter the mobility of the plasmid. The results suggest a lack of interaction with DNA for compounds **1–2** as compared to cisplatin, which induces the retention of plasmid migration in a dose-dependent manner. Thus, the mechanism of cell death observed for **1–2** does not seem to be triggered by DNA interaction.

Conclusions

Complexes $[\{RuCp(PPh_3)_2$-μ-dmoPTA-1κ*P*:2κ^2-*N*,*N*′-CuCl$\}_2$-μ-Cl-μ-$OCH_3](CF_3SO_3)_2\cdot(CH_3OH)_4$ (**1**) and $[\{RuCp(PPh_3)_2$-μ-dmoPTA-1κ*P*:2κ^2-*N*,*N*′-NiCl$\}_2$-μ-Cl-μ-OH$](CF_3SO_3)_2$ (**2**) have been synthesized and characterized by NMR, IR, elemental analysis and single-crystal X-ray. And their subsequent transformation in the respective heterobimetallic complexes was demonstrated. These complexes have shown activity in the range of 20–41 nM, confirming an enhancement in antiproliferative activity to the most active heterometallic complexes previously synthesized by us, establishing the known most active anticancer transition metal complexes to the best of our knowledge. Deepening on the mechanism of action of the compounds, both have been studied in different assays such as colony formation assay for SW1573 cells, where the presence of the two complexes means a decrease in the size and density of colonies, cell death mechanism assay for HeLa cells where both complexes induce apoptosis, with complex **2** causing faster apoptosis than complex **1** and their interaction with pBR322 DNA plasmid was also evaluated where it was observed that none of the compounds modified the mobility of the plasmid, suggesting that its mechanism of action is different from that of cisplatin. Natural metalloenzymes containing more than one metal are a paradigmatic example of efficiency, mostly due to their multi-metallic composition that provides a cooperative single-molecule platform for multi-step catalytic reactions. Additional essays are in progress to determine the biological target of the complexes and how they interact with the cancer cells. Synthesis of new heterometallic complexes is also in progress both to obtain more active antiproliferative compounds and to determine the structure factors and chemical properties that provide their activity.

Author contributions

Characterization and stability tests of the complexes A. A., F. S., Z. M., P. L. and A. R. contributed to the synthesis. The biological assays were performed by A. P., A. G. and J. M. P. A. R. and J. M. P. contributed to the obtention of the funds. All the authors contributed equally to writing the manuscript.

Conflicts of interest

There are no conflicts to declare.

Acknowledgements

The authors thank Junta de Andalucía for the FEDER project PY20_00791, PAI group FQM-317 and the University of Almería for the project UAL2020-RNM-B2084 (co-funded by European Commission FEDER program). Andrés Alguacil thanks PY20_00791 for a research contract. Authors from BioLab thank the Spanish Government (project PID2021-123059OB-I00 funded by MCIN/AEI/10.13039/501100011033/FEDER, UE). A. P. thanks the EU Social Fund (FSE) and the Canary Islands ACIISI for a predoctoral grant TESIS2020010055.

References

1 B. Rosenberg, L. Van Camp and T. Krigas, *Nature*, 1965, **205**, 698–699.
2 P. Heffeter, U. Jungwirth, M. Jakupec, C. Hartinger, M. Galanski, L. Elbling, M. Micksche, B. Keppler and W. Berger, *Drug Resistance Updates*, 2008, **11**, 1–16.
3 E. S. Antonarakis and A. Emadi, *Cancer Chemother. Pharmacol.*, 2010, **66**, 1–9.
4 E. Alessio and L. Messori, *Molecules*, 2019, **24**, 1995.
5 C. S. Allardyce, P. J. Dyson, D. J. Ellis and S. L. Heath, *Chem. Commun.*, 2001, 1396–1397.
6 M. Rausch, P. J. Dyson and P. Nowak-Sliwinska, *Adv. Ther.*, 2019, **2**, 1900042.
7 A. D. Phillips, L. Gonsalvi, A. Romerosa, F. Vizza and M. Peruzzini, *Coord. Chem. Rev.*, 2004, **248**, 955–993.

8 J. Bravo, S. Bolaño, L. Gonsalvi and M. Peruzzini, *Coord. Chem. Rev.*, 2010, **254**, 555–607.
9 A. Guerriero, M. Peruzzini and L. Gonsalvi, *Coord. Chem. Rev.*, 2018, **355**, 328–361.
10 F. Scalambra, P. Lorenzo-Luis, I. de los Ríos and A. Romerosa, *Eur. J. Inorg. Chem.*, 2019, 1529–1538.
11 L. Hajji, C. Saraiba-Bello, G. Segovia-Torrente, F. Scalambra and A. Romerosa, *Eur. J. Inorg. Chem.*, 2019, 4078–4086.
12 A. Mena-Cruz, P. Lorenzo-Luis, A. Romerosa, M. Saoud and M. Serrano-Ruiz, *Inorg. Chem.*, 2007, **46**, 6120–6128.
13 A. Mena-Cruz, P. Lorenzo-Luis, A. Romerosa and M. Serrano-Ruiz, *Inorg. Chem.*, 2008, **47**, 2246–2248.
14 A. Mena-Cruz, P. Lorenzo-Luis, V. Passarelli, A. Romerosa and M. Serrano-Ruiz, *Dalton Trans.*, 2011, **40**, 3237–3244.
15 M. Serrano-Ruiz, L. M. Aguilera-Sáez, P. Lorenzo-Luis, J. M. Padrón and A. Romerosa, *Dalton Trans.*, 2013, **42**, 11212–11219.
16 Z. Mendoza, P. Lorenzo-Luis, M. Serrano-Ruiz, E. Martín-Batista, J. M. Padrón, F. Scalambra and A. Romerosa, *Inorg. Chem.*, 2016, **55**, 7820–7822.
17 Z. Mendoza, P. Lorenzo-Luis, F. Scalambra, J. M. Padrón and A. Romerosa, *Dalton Trans.*, 2017, **46**, 8009–8012.
18 Z. Mendoza, P. Lorenzo-Luis, F. Scalambra, J. M. Padrón and A. Romerosa, *Eur. J. Inorg. Chem.*, 2018, 4684–4688.
19 M. C. Linder, *Biochemistry of Copper*, 1991, pp. 1–13.
20 D. L. Huffman and T. V. O'Halloran, *Annu. Rev. Biochem.*, 2001, **70**, 677–701.
21 T. Wang and Z. Guo, *Curr. Med. Chem.*, 2006, **13**, 525–537.
22 N. E. Dixon, C. Gazzola, R. L. Blakeley and B. Zerner, *J. Am. Chem. Soc.*, 1975, **97**, 4131–4133.
23 H. C. Shih, N. Tang, C. J. Burrows and S. E. Rokita, *J. Am. Chem. Soc.*, 1998, **120**, 3284–3288.
24 C. J. Burrows and S. E. Rokita, *Acc. Chem. Res.*, 1994, **27**, 295–301.
25 A. Mena-Cruz, P. Lorenzo-Luis, V. Passarelli, A. Romerosa and M. Serrano-Ruiz, *Dalton Trans.*, 2011, **40**, 3237–3244.
26 D. Nieto, A. M. González-Vadillo, S. Bruña, C. J. Pastor, C. Ríos-Luci, L. G. León, J. M. Padrón, C. Navarro-Ranninger and I. Cuadrado, *Dalton Trans.*, 2011, **41**, 432–441.
27 M. K. Mohamed Subarkhan, L. Ren, B. Xie, C. Chen, Y. Wang and H. Wang, *Eur. J. Med. Chem.*, 2019, **179**, 246–256.
28 J. Ruiz, C. Vicente, C. De Haro and A. Espinosa, *Inorg. Chem.*, 2011, **50**, 2151–2158.
29 A. Yamamoto, R. Honma and M. Sumita, *J. Biomed. Mater. Res.*, 1998, **39**, 331–340.
30 A. Yamamoto, R. Honma, A. Tanaka and M. Sumita, *J. Biomed. Mater. Res.*, 1999, **47**, 396–403.
31 M. F. Primik, G. Mühlgassner, M. A. Jakupec, O. Zava, P. J. Dyson, V. B. Arion and B. K. Keppler, *Inorg. Chem.*, 2010, **49**, 302–311.
32 N. F. B. Azeredo, F. V. Borges, M. S. Mathias, J. A. L. C. Resende, R. W. A. Franco, M. M. Kanashiro, A. Horn and C. Fernandes, *BioMetals*, 2021, **34**, 229–244.
33 C. Ríos-Luci, L. G. León, A. Mena-Cruz, E. Pérez-Roth, P. Lorenzo-Luis, A. Romerosa and J. M. Padrón, *Bioorg. Med. Chem. Lett.*, 2011, **21**, 4568–4571.